Inorg. Chem. **2007**, *46*, 2744–2750

Synthesis, Crystal Structure, and Microstructure Analysis of Perovskite-Type Compounds $LnCo_{0.95}Ni_{0.05}O_3$ (Ln = La, Pr, Nd, Sm, Gd, and Dy)

M. H. Aguirre,* R. Robert, D. Logvinovich, and A. Weidenkaff

Empa, Swiss Federal Laboratories for Materials Testing and Research, Solid State Chemistry and Catalysis, Ueberlandstr. 129, CH-8600 Dübendorf, Switzerland

Received December 13, 2006

The crystal structure and the microstructure of $LnCo_{0.95}Ni_{0.05}O_3$ compounds, synthesized by a soft chemistry process, were studied. Synchrotron and laboratory X-ray diffraction data of $LnCo_{0.95}Ni_{0.05}O_3$ (Ln = Pr, Nd, Sm, Gd, and Dy) can be refined in the *Pbnm* space group (SG). The orthorhombic symmetry has been confirmed by transmission electron microscopy. The X-ray diffraction data of $LaCo_{0.95}Ni_{0.05}O_3$ can be fitted with rhombohedral $R\bar{3}c$ and monoclinic $I2/a$ SG. The comparison of experimental electron diffraction with theoretical simulation showed the monoclinic symmetry for the La compound has a better match than that of the rhombohedral symmetry. The Pr compound has shown to have a three-dimensional microdomain texture in which the orientation of the real unit cell, i.e., $\sim\sqrt{2}a_p \times \sqrt{2}a_p \times 2a_p$ (where a_p is the lattice parameter of the aristotype $Pm\bar{3}m$ perovskite, noted with a "p" subscript), alternates in each domain in one of the three space directions.

Introduction

Lanthanum cobaltates are ABO_3-type perovskites that show interesting catalytic, magnetic, and semiconducting properties for industrial applications. They are considered for use as cathode materials in solid oxide fuel cells due to their high electrical and ionic (O^{2-}) conductivities, as oxygen permeable membranes, as catalysts for the oxidation of the CO, for NO_x decomposition, and for the combustion of methane and propane.[1] They also attracted attention in the field of sustainable and renewable energy, since they are suitable for thermoelectric power applications due to their high thermal and oxidizing stability at medium and high working temperatures.[2] Cobalt oxide materials are considered as potential thermoelements due to their high thermopower values and semiconducting-like behavior. The electrical properties determined by the power factor, defined as S^2/ρ (S is the Seebeck coefficient, ρ the electrical resistivity), can be fine-tuned by suitable substitutions. Our previous studies[3] showed the effect of Ni for a low substitution level into the $LaCoO_3$ system. A substantial decrease of electrical resistivity, while the large Seebeck coefficient values were kept, was observed. The room-temperature crystal structure of $LaCoO_3$ was reported as the rhombohedral $R\bar{3}c$ space group (SG)[3,4] and $LnCoO_3$ (Ln = other rare earth or yttrium cations) in the orthorhombic *Pbnm* SG.[5] Recently, a cooperative Jahn−Teller (JT) distortion of the CoO_6 octahedra was detected in $LaCoO_3$[6] by high-resolution synchrotron X-ray diffraction of a single crystal and from infrared spectroscopy.[7] The presence of JT distortion in $LaCoO_3$ is not incompatible with rhombohedral symmetry, and the JT distortion would explain the intermediate spin state of the Co^{3+} in the structure.

The syntheses by soft chemistry routes are very suitable for the production of transition metal oxides phases with high surface area and diverse composition, especially for low-level substitution which cannot be obtained by a classical solid-state reaction synthesis. The combination of synchrotron X-ray diffraction and transmission electron microscopy

* To whom correspondence should be addressed. Tel: +41 44 823 4689. Fax: +41 44 823 4034. E-mail: myriam.aguirre@empa.ch.

(1) Mitchell, R.H. *Perovskites: Modern and Ancient*; Almaz Press: Thunder Bay, ON, Canada 2002.
(2) Robert, R.; Romer, S.; Reller, A.; Weidenkaff, A. *Adv. Eng. Mater.* **2005**, *7*, 303−308.
(3) Robert, R.; Bocher, L.; Trottmann, M.; Reller, A.; Weidenkaff, A. *J. Solid State Chem.* **2006**, *179*, 3893−3899.
(4) Walmsley, J.; Bardal, A.; Kleveland, K.; Einarsrud, M.-A.; Grande, T. *J. Mater. Sci.* **2000**, *35*, 4251−4260.
(5) Knížek, K.; Jirák, Z.; Hejtmánek, J.; Veverka, M.; Maryško, M.; Maris, G.; Palstra, T. *Eur. Phys. J. B* **2005**, *47*, 213−220.
(6) Maris, G.; Ren, Y.; Volotchaev, V.; Zobel, C.; Lorenz, T.; Palstra, T. *Phys. Rev. B: Condens. Matter Mater. Phys.* **2003**, *67*, 224423.
(7) Yamaguchi, S.; Okimoto, Y.; Tokura, Y. *Phys. Rev. B: Condens. Matter Mater. Phys.* **1997**, *55*, 8666−8669.

10.1021/ic0623821 CCC: $37.00
Published on Web 03/08/2007

(TEM) is very powerful as a characterization technique to investigate subtle structural variations and the microstructure of the perovskite materials with this low-level substitution.

In this paper we report the influence of the different lanthanide ionic radii in the $LnCo_{0.95}Ni_{0.05}O_3$ system on the crystal structure. We synthesized $LnCo_{0.95}Ni_{0.05}O_3$ (Ln = La, Pr, Nd, Sm, Gd, and Dy) compounds by a soft chemistry route using citrate complexes as precursors and characterized them by synchrotron powder X-ray diffraction (SPXRD) and TEM. Structural parameters obtained by Rietveld refinement from SPXRD data are used to perform theoretical simulation of the electron diffraction (ED) and high-resolution electron microscopy (HREM) image. The comparison of the experimental image and ED with the theoretical simulation allows one to analyze the validity of the structural model and avoid the influence of the microstructure on the space group assignment.

Experimental Section

Fine powders with the composition $LnCo_{0.95}Ni_{0.05}O_3\pm_\delta$ (Ln = La, Pr, Nd, Sm, Gd, and Dy) were obtained by thermal decomposition of the corresponding amorphous citrate precursors. The formation of the perovskite phases from water soluble precursors is described elsewhere.[2,8] Precursors for the $LaCo_{1-x}Ni_xO_{3\pm\delta}$ compositions were prepared from an aqueous solution containing stoichiometric amounts of dissolved $Ln(NO_3)_3{\cdot}6H_2O$ (Merck, ≥97%), $Co(NO_3)_2{\cdot}6H_2O$ (Merck, ≥97%), and $Ni(NO_3)_2{\cdot}6H_2O$ (Merck, ≥99%). An excess of the chelating agent, citric acid (Sigma-Aldrich), was added to the metal salt solutions under continuous stirring at room temperature to prevent precipitation. The citric acid to metal ion ratio was 2:1. Homogeneous clear solutions were obtained after heating and polymerization under reflux for 3 h at T = 553 K. The precursor solutions were dried using a rotary evaporator (T = 333 K, p = 20 mbar) to promote the formation of pink-transparent viscous gels. Every gel was predecomposed at T = 573 K, resulting in a voluminous product which was then milled and calcinated at T = 973 K for Ln = La, Pr, Nd, Sm, and Gd and T = 1073 K for Ln = Dy, during 6 h in ambient atmosphere to obtain the pure perovskite $LnCo_{0.95}Ni_{0.05}O_3\pm_\delta$ phases.

All samples were routinely checked for purity and crystallinity by X-ray diffraction using a Philips X'Pert PRO MPD Θ−Θ system equipped with a linear detector (X'Celerator). SPXRD data for refinement were collected on the B2 line at HasyLab (Hamburg, Germany) using a wavelength of 0.49588 Å, working in transmission mode. Structural refinements were performed using the FULLPROF program.[9]

The elemental compositions of the samples were analyzed by energy dispersive X-ray spectrometry (EDXS-Link Pentafet 5947, from Oxford Microanalysis group) while TEM measurements were performed (in situ measurements) by a Jeol JEM FX2000 and 3000EX-FEG. The oxygen content was determined by the hot gas-extraction method (HGE) using a LECO TC500 analyzer and the thermogravimetry (TGA) hydrogen reduction method using a Netzsch STA 409 CD thermobalance. For the hot gas-extraction method, a small aliquot of sample (ca. 15 mg) was placed in a tin container. This container was positioned in a double-graphite crucible and heated to 3273 K, which results in a carbothermal reduction of the sample. The lattice oxygen reacted with carbon from the crucible to form CO and later CO_2 by a catalytic process. The oxygen content of the samples was determined from the evaluated CO_2 measured by using an infrared detector. Silicon oxide was used as an oxygen calibration standard. Thermogravimetric reductions were performed by heating the samples up to T = 1223 K with a heating rate of 2 K/min under 20% H_2 in He atmosphere. In these conditions, the sample is reduced to lanthanum oxide, cobalt, and nickel metals, as shown in eq 1. The oxygen content of the starting compound can be calculated from the recorded weight loss versus temperature and the determination of reduction product composition.

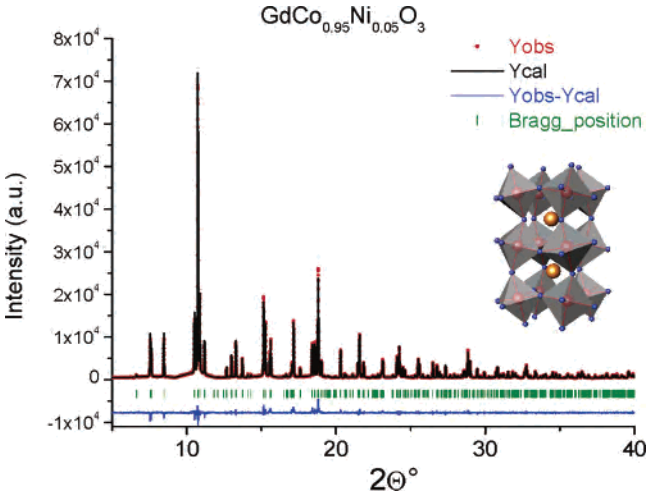

Figure 1. An example of the Rietveld SPXRD pattern for $GdCo_{0.95}Ni_{0.05}O_3$. The present data were collected at room temperature. Vertical tick marks indicate the position of allowed Bragg peaks in the *Pbnm* space group. A model of the structure designed by ATOMS software can be seen inserted in the pattern.

$$LnCo_{0.95}Ni_{0.05}O_{3\pm\delta} + (1.5+\delta)H_2 \rightarrow 0.5Ln_2O_3 + 0.95Co + 0.05Ni + (1.5+\delta)H_2O \quad (1)$$

The structure and microstructure studies were done by high-resolution transmission electron microscopy and electron diffraction in a Jeol JEM 3000EX field emission gun microscope and a Philips CM30 with a thermoionic gun. The JEMS program[10] was used to perform the high-resolution image and diffraction simulation.

Results and Discussion

I. Analysis of the SPXRD Data. The SPXRD data in Figure 1 as well as laboratory X-rays show a single phase for the $LnCo_{0.95}Ni_{0.05}O_{3\pm\delta}$ systems (Ln = La, Nd, Pr, Sm, Gd, and Dy). The reflections can be indexed, similar to the series $LnCoO_3$, in an orthorhombic unit cell (noted with "o" subscript in every vector) with *Pbnm* SG,[5] and with parameters $a \approx b \approx a_p\sqrt{2}$, $c \approx 2a_p$, except for the La system or $LaCoO_3$.[11] SPXRD data of $LaCo_{0.95}Ni_{0.05}O_{3\pm\delta}$ can be fitted using both structural models, in the rhombohedral with $R\bar{3}c$ SG, $a \approx a_p\sqrt{2}$ and $\alpha \approx 60.82°$, as well as in the monoclinic structure ($a \approx b \approx a_p\sqrt{2}$, $c \approx 2a_p$) with $I2/a$ SG. This apparently contradictory result has also reported

(8) Krupicka, E.; Reller, A.; Weidenkaff, A. *Cryst. Eng.* **2002**, *5*, 195−202.
(9) Rodríguez-Carvajal, J. *Physica B: Condensed Matter (Amsterdam, Neth.)* **1993**, *192*, 55−69.
(10) Stadelmann, P. A. *Ultramicroscopy* **1987**, *21*(2), 131−145.
(11) Radaelli, P.; Cheong, S.-W. *Phys. Rev. B: Condens. Matter Mater. Phys.* **2002**, *66*, 094408.

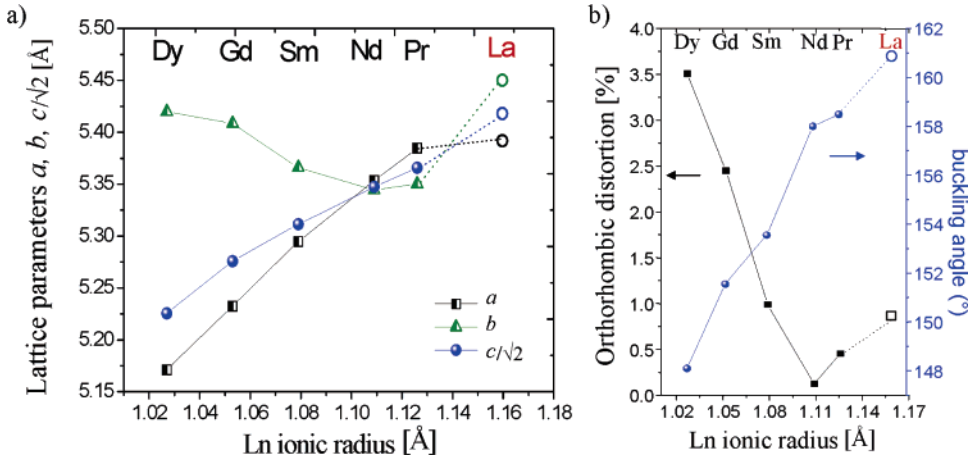

Figure 2. (a) Lattice parameter vs ionic radii of Ln. (b) Orthorhombic distortion and M−O(I)−M angle (buckling angle) vs ionic radii of Ln.

Table 1. Refined Cell Parameters, Volume, R_{wp}, R_p, and χ from SPXRD Data

$LnCo_{0.95}Ni_{0.05}O_{3\pm\delta}$	a (Å)	b (Å)	c (Å)	V (Å^3)	R_{wp}	R_p	χ^2
La (monoclinic $I2/a$) $\beta = 90.998(8)$ deg	5.381(1)	5.449(7)	7.665(1)	224.994(1)	14.2	10.6	1.95
La (rhombohedral $R3c$) $\alpha = \beta = \gamma =$ 60.817(5) deg		5.447(1)		337.361(2)	10.4	14.2	1.98
Pr	5.384(7)	5.350(2)	7.588(4)	216.380(3)	8.54	15.5	2.16
Nd	5.353(7)	5.344(4)	7.562(5)	216.380(6)	6.76	12.0	2.55
Sm	5.294(7)	5.366(1)	7.511(6)	213.411(7)	7.29	13.5	1.83
Gd	5.232(4)	5.408(6)	7.461(1)	211.148(8)	8.11	17.1	1.65
Dy	5.171(1)	5.419(9)	7.391(1)	207.102(3)	13.9	11.1	1.81

for the $LaCoO_3$ compound[6,11,12] from powder and single-crystal diffraction data. It is possible that very small monoclinic distortions are not detectable from powder XRD data. (See section II, TEM Structure, Microstructure, and Composition, for more details.)

The calculated lattice parameters, unit cell volume, and agreement factors are summarized in Table 1 for all compounds. The evolution of the lattice parameters with the different Ln^{3+} ionic radius for compounds with orthorhombic structure is shown in Figure 2a. The $b > c/\sqrt{2} > a$ relation is observed from Dy to Sm compounds (so-called O-type structure), whereas $a > c/\sqrt{2} > b$ relation is observed for Nd and Pr. It is useful to calculate the orthorhombic distortion for Ln compounds to explain this tendency, which is defined as a standard deviation divided by the lattice parameter average in eq 2

$$\text{dist}_{\text{orth}} = \frac{\sqrt{\sum (a_i - \bar{a})^2}}{\bar{a}} \qquad (2)$$

where $a_i = a$, b, and $c/\sqrt{2}$ and $\bar{a}$ is the average of a_i, displayed in Figure 2b. The orthorhombic distortion decreases from the Dy to the Nd compounds and increases again for the Pr compound, passing through the minimum value for Nd compound, where $a \approx b \approx c/\sqrt{2}$. Additionally, the M−O(I)−M angle (or the so-called buckling angle, M = metal ions) increases with the ionic radius of the lanthanide (Figure 2b). The distortion of the MO_6 octahedra is also clearly seen in the deviation of the O(I)−M−O(II) angle from 90°. The deviations are around 0.5, 0.95, 0.67, and 1.55% for Nd, Sm, Gd, and Pr compounds, respectively. The relationship between lattice distortion, buckling angle, and MO_6 octahedra distortion plays an important role in the different microstructure found in these compounds. (See TEM Structure, Microstructure, and Composition below for more details.) It is also worth mentioning that Ln compounds present MO_6 octahedra with basal-plane distortion, i.e., two different bond lengths for M−O(II) in the basal plane. This distortion is known as JT Q_2 type (or antiferrodistorsive).[13]

The size of the Ln atoms modifies the bending of M−O−M bond and the strength of the integral hopping between e_g orbitals (e_g(M)−p_σ−e_g(M)) and, therefore, the electronic bandwidth.[14] Both the orthorhombic lattice distortion and buckling angle are greater for $LnCo_{0.95}Ni_{0.05}O_{3\pm\delta}$ compared with the values for the homologous series of $LnCoO_3$;[6] this can be explained with the different Ni and Co atomic radii.

II. Tem Studies of Structure, Microstructure, and Composition. The ED and HREM studies were done to confirm the refined structural model from SPXRD data. EDXS measurements, done in situ TEM (Table 3), revealed a cation ratio of $La_{0.99\pm0.02}Co_{0.95\pm0.02}Ni_{0.05\pm0.015}$ in good agreement with the nominal stoichiometry within the experimental error. The anionic composition evaluated by HGE and TGA shows small oxygen deficiency for all samples

(12) Haas, O.; Struis, R. P.; McBreen, J. M. *J. Solid State Chem.* **2004**, *177*, 1000−1010.

(13) García-Muñoz, J. L.; Suaaidi, M.; Fontcuberta, J.; Rodríguez-Carvajal, J. *Phys. Rev. B: Condens. Matter Mater. Phys.* **1997**, *55*, 34−37.

(14) Hwang, H. Y.; Cheong, S-W.; Radaelli, P. G.; Marezio, M.; Batlogg, B. *Phys. Rev. Lett.* **1995**, *75*, 914−917.

Table 2. Refined Fractional Atomic Position of $LnCo_{0.95}Ni_{0.05}O_3$ from SPXRD; $0.07(1) < B_{iso}$ (Å^2) $< 1.50(5)$

		La						
$LnCo_{0.95}Ni_{0.05}O_{3\pm\delta}$	position	$R\bar{3}c$	$I2/a$	Pr	Nd	Sm	Gd	Dy
Ln	*x*	0.2545(4)	0.25	0.0053(3)	−0.0064(3)	0.9930(2)	0.9870(1)	0.9830(5)
	y	0.5124(1)	0.2498(4)	0.0288(9)	0.0351(9)	0.0474(1)	0.0586(3)	0.0655(6)
	z	0.2330(4)	0	0.25	0.25	0.25	0.25	0.25
M = Co, Ni	*x*	0	0.75	0.5	0.5	0.5	0.5	0.5
	y	0	0.25	0	0	0	0	0
	z	0	0.25	0	0	0	0	0
O(I)	*x*	0.1253(2)	0.25	0.934(2)	0.066(3)	0.0834(2)	0.0851(1)	0.0960(7)
	y	0.4530(7)	0.7003(3)	0.4888(1)	0.4925(1)	0.4869(1)	0.4809(1)	0.4669(6)
	z	0.7065(2)	0	0.25	0.25	0.25	0.25	0.25
O(II)	*x*		0.0168(4)	0.7049(1)	0.7181(2)	0.7077(1)	0.7021(9)	0.7006(1)
	y		0.0159(4)	0.2904(1)	0.2871(2)	0.2941(1)	0.2972(8)	0.2969(1)
	z		0.2147(3)	0.0221(1)	0.0364(1)	0.0386(2)	0.0455(6)	0.0490(9)
distortion angle (deg)	M−O(I)−M		160.90(2)	158.49(8)	158.70(1)	153.21(9)	152.46(6)	148.11(1)
	M−O(II)−M		161.20(5)	158.20(3)	157.30(4)	153.92(3)	150.63(19)	149.56(3)
bond distances (Å)	M−O(I)		1.943(5)	1.9310(2)	1.924(3)	1.930(2)	1.9205(1)	1.922(2)
	M−O(II)		1.952(1)	1.952(8)	1.948(1)	1.945(7)	1.954(4))	1.949(7)
			1.931(1)	1.913(8)	1.910(1)	1.924(7)	1.936(5	1.934(7)

$LnCo_{0.95}Ni_{0.05}O_{3\pm\delta}$	position	La (*I*2/*a*)	Pr	Nd	Sm	Gd	Dy
Ln	*x*	0.25	0.0053(3)	−0.0064(3)	0.9930(2)	0.9870(1)	0.9830(5)
	y	0.2498(4)	0.0288(9)	0.0351(9)	0.0474(1)	0.0586(3)	0.0655(6)
	z	0	0.25	0.25	0.25	0.25	0.25
M = Co, Ni	*x*	0.75	0.5	0.5	0.5	0.5	0.5
	y	0.25	0	0	0	0	0
	z	0.25	0	0	0	0	0
O(I)	*x*	0.25	0.934(2)	0.066(3)	0.0834(2)	0.0851(1)	0.0960(7)
	y	0.7003(3)	0.4888(1)	0.4925(1)	0.4869(1)	0.4809(1)	0.4669(6)
	z	0	0.25	0.25	0.25	0.25	0.25
O(II)	*x*	0.0168(4)	0.7049(1)	0.7181(2)	0.7077(1)	0.7021(9)	0.7006(1)
	y	0.0159(4)	0.2904(1)	0.2871(2)	0.2941(1)	0.2972(8)	0.2969(1)
	z	0.2147(3)	0.0221(1)	0.0364(1)	0.0386(2)	0.0455(6)	0.0490(9)
distortion angle (deg)	M−O(I)−M	160.90(2)	158.49(8)	158.70(1)	153.21(9)	152.46(6)	148.11(1)
	M−O(II)−M	161.20(5)	158.20(3)	157.30(4)	153.92(3)	150.63(19)	149.56(3)
bond distances (Å)	M−O(I)	1.943(5)	1.9310(2)	1.924(3)	1.930(2)	1.9205(1)	1.922(2)
	M−O(II)	1.952(1)	1.952(8)	1.948(1)	1.945(7)	1.954(4)	1.949(7)
		1.931(1)	1.913(8)	1.910(1)	1.924(7)	1.936(5)	1.934(7)

Table 3. Cationic Composition and Oxygen Content of Ln Compounds

	cationic composition/EDXS		oxygen content	
elemental composition	Co	Ni	hot gas extraction	thermogravimetry (He/H_2 80:20)
$LaCo_{0.95}Ni_{0.05}O_{3\pm\delta}$	0.95 ± 0.02	0.054 ± 0.015	2.98 ± 0.02	2.97 ± 0.09
$NdCo_{0.95}Ni_{0.05}O_{3\pm\delta}$	0.95 ± 0.02	0.052 ± 0.015	2.99 ± 0.02	2.99 ± 0.07
$PrCo_{0.95}Ni_{0.05}O_{3\pm\delta}$	0.96 ± 0.02	0.048 ± 0.015	3.08 ± 0.05	3.13 ± 0.05
$SmCo_{0.95}Ni_{0.05}O_{3\pm\delta}$	0.95 ± 0.02	0.053 ± 0.015	3.01 ± 0.01	2.96 ± 0.03
$GdCo_{0.95}Ni_{0.05}O_{3\pm\delta}$	0.96 ± 0.02	0.051 ± 0.015	3.02 ± 0.02	2.96 ± 0.06
$DyCo_{0.95}Ni_{0.05}O_{3\pm\delta}$	0.95 ± 0.02	0.049 ± 0.015	2.99 ± 0.01	3.04 ± 0.06

except the Pr compound that shows an excess of oxygen (see Table 3).

$LaCo_{0.95}Ni_{0.05}O_3$. As it was mentioned before, the SPXRD data of the $LaCo_{0.95}Ni_{0.05}O_3$ compound can be refined with rhombohedral or monoclinic symmetries, both giving similar accordance factors. To distinguish between those structures, several ED zone axes were simulated with both models by JEMS software and compared with the experimental ones. We found some discrepancies between the rhombohedral $[001]_R$ simulated ED in Figure 3a and the experimental ED in Figure 3c. The extra reflections $\pm(011)_M$ and $\pm(0{-}11)_M$ in Figure 3b (subscript M = monoclinic) are permitted in the monoclinic *I*2/*a* SG, but the reflections $\pm(0,2n{+}1,0)_R$ and $\pm(2n{+}1,0,0)_R$ (that should appear at the same position as $\pm n(0{-}11)_M$ and $\pm n(011)_M$) are not allowed in rhombohedral $R\bar{3}c$ SG, as seen in the ED simulation of Figure 3a. These reflections were carefully checked to ensure that they did not arise because of multiple scattering. The experimental ED can be indexed with $[100]_M$, seen in Figure 3b, where the micrograph was taken in saturated mode for enhancing the reflections $\pm(011)_M$ and $\pm(0{-}11)_M$. Figure 4 shows the diffraction pattern along the $[001]_M$ zone axis and the corresponding HREM image with the theoretical simulation inset. We found good agreement between the experimental and the simulated image by JEMS in the monoclinic model (*I*2/*a* SG, for simulation conditions see the figure caption).

The most important difference between rhombohedral ($R\bar{3}c$) and monoclinic (*I*2/*a*) structures (both distorted from parent cubic perovskite) is the appearance of two different Co−O bond lengths in the second structure. The monoclinic *I*2/*a* SG is a subgroup of $R\bar{3}c$ (highest symmetry). It is very difficult to distinguish between them, because of the small difference in Co−O(I) and Co−O(II) lengths (see Table 2). The monoclinic symmetry can accommodate not only the

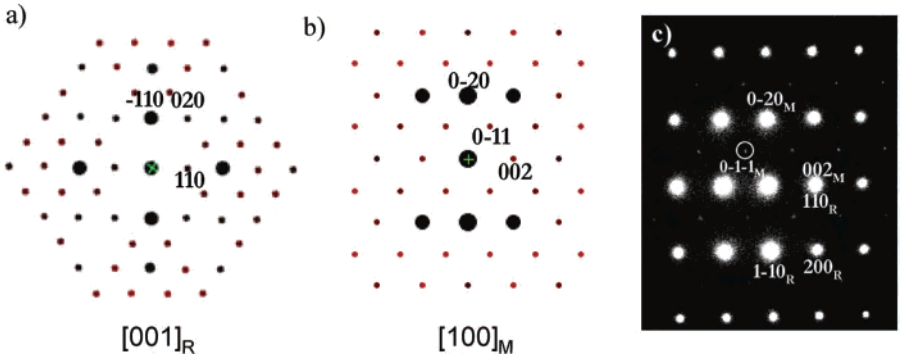

Figure 3. Diffraction analysis of $LaCo_{0.95}Ni_{0.05}O_3$. (a) Simulated ED pattern in the rhombohedral $R\bar{3}c$ SG, [001] zone axis. (b) Simulated ED pattern in the monoclinic $I2/a$ SG, [100] zone axis. (c) Experimental ED pattern showing extra reflections belonging to monoclinic symmetry.

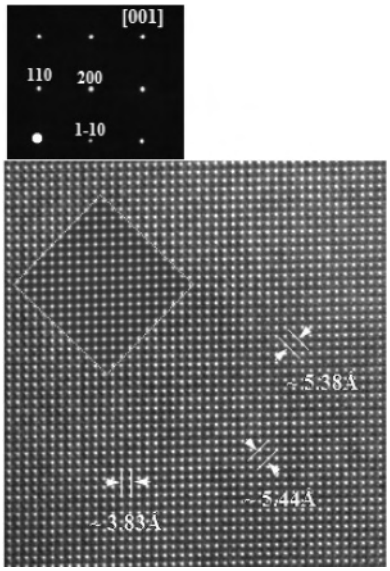

Figure 4. ED and HREM of $LaCo_{0.95}Ni_{0.05}O_3$ in [001] zone axis, with simulated image inset in monoclinic model (thickness (th) = 5 nm and Δdefocus = −45 nm (Δ*f*)).

rotation of octahedra but also the different bond lengths of Co−O. These different bond lengths are induced by the coherent Jahn−Teller distortion, which would explain the intermediate spin state in the analogous $LaCoO_3$ system.[6]

$LnCo_{0.95}Ni_{0.05}O_3$ (Ln = Dy, Gd, Sm, and Nd). ED and HREM analyses of the Dy, Gd, Sm, and Nd compounds show an orthorhombic structure, as presented in the Rietveld refinement. The common ED pattern from the $[110]_o$ zone axis of these compounds is shown in Figure 5a. This zone axis can be related to the cubic perovskite as $[110]_o \leftrightarrow [010]_p$. The presence of the 00*l* reflections, with $l = 2n$, which are forbidden for the space group *Pbnm*, on the $[110]_o$ diffraction pattern is due to double diffraction. Parts b and c of Figure 5 show the HREM image of the same zone axis for the Sm and Gd compounds, respectively. The different contrast displayed by both micrographs is due to the different microscopes used for the analysis (with a different gun type); that in Figure 5b corresponds to the Philips CM30 with LaB_6 and that in Figure 5c corresponds to the Jeol JEM 3000EX with a field emission gun. The models of the structure for every compound, obtained by Rietveld refinement, were used to make the HREM simulation and took into account the different microscope types. For the $SmCo_{0.95}Ni_{0.05}O_3$ compound, the image simulation can be seen inserted into micrograph of Figure 5b, and for the $[110]_o$ zone axis of the Gd compound, the image simulation can be seen inserted into the micrograph of Figure 5c. Parts a and b of Figure 6 show ED and HREM images for the Gd compound of $[101]_o$ and $[010]_o$ zone axes, respectively. It is possible to observe weak $\pm(0,2n+1,0)$ reflections in $[101]_o$ that are not allowed in *Pbnm* SG, but appear for double diffraction. High-resolution image simulations inserted into the micrographs

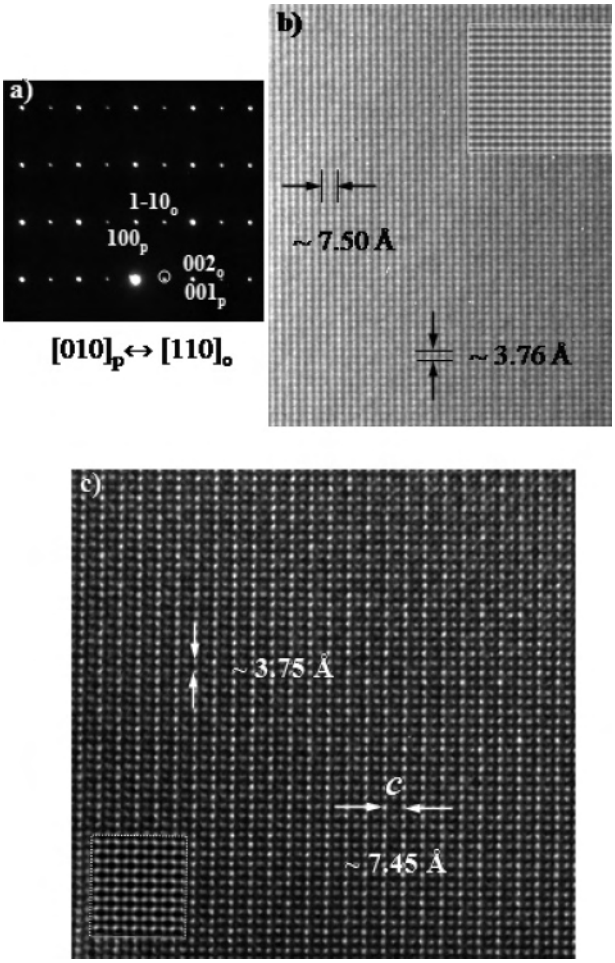

Figure 5. (a) Usual ED pattern of $[110]_o \leftrightarrow [010]_p$ for $LnCo_{0.95}Ni_{0.05}O_3$ (Ln = Pr, Nd, Sm, Gd, and Dy) with orthorhombic structure. (b) HREM of $[110]_o$ zone axis for Sm compound with theoretical simulation inset (th = 9 nm, $\Delta f = -10$ nm). (c) HREM same zone axis for Gd compound with theoretical simulation inset (th = 15 nm, $\Delta f = -10$ nm).

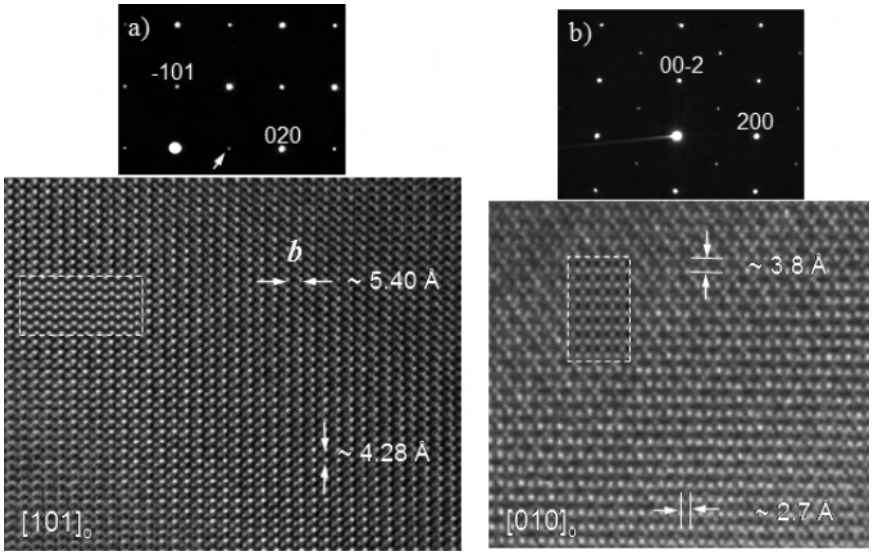

Figure 6. ED, HREM, and theoretical simulation inset of Gd compound. (a) $[101]_o$ Zone axis, th = 8 nm, $\Delta f = 10$ nm. (b) $[111]_o$ Zone axis, th = 5 nm, $\Delta f = -2$ nm.

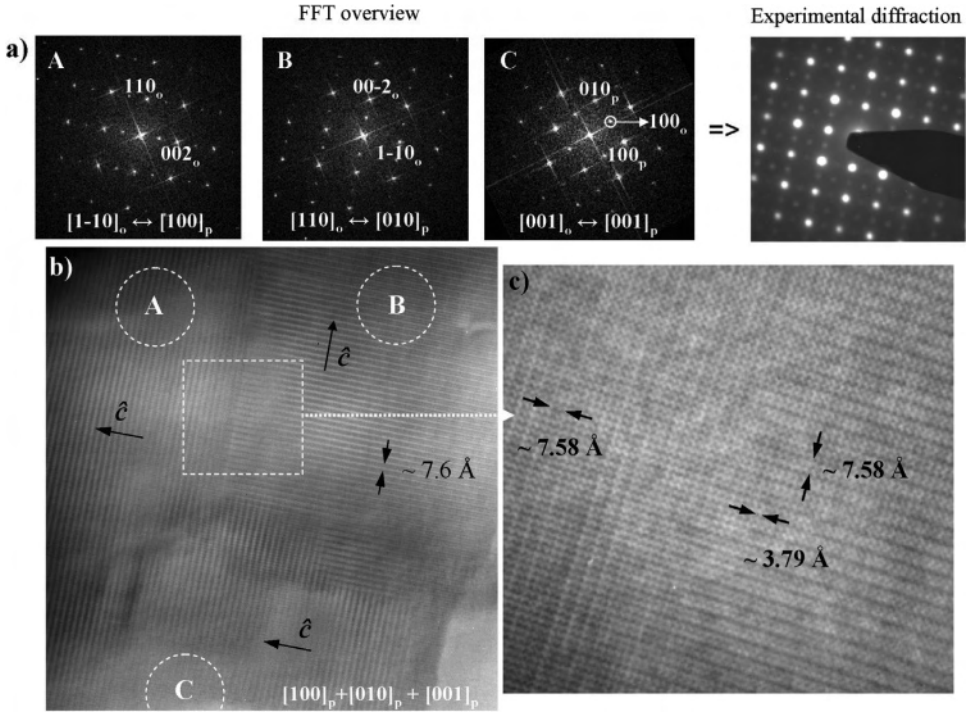

Figure 7. FFT, ED, and HREM of $PrCo_{0.95}Ni_{0.05}O_3$. (a) FFT of each twin domain of A, B, and C indicated in part b HREM and the experimental ED showing the diffraction of twin domains overlapping. (b) Medium-resolution image of twin domains showing the $\hat{c}$ axis ($c \sim 2a_p \sim 7.6$ Å) distributed in the three space orientations. (c) Enlarged region highlights details of the supercell.

present good agreement with the experimental image. This complementary TEM data supports the correctness of the atomic model for the compounds with orthorhombic structure.

$PrCo_{0.95}Ni_{0.05}O_3$. The analysis of the $PrCo_{0.95}Ni_{0.05}O_3$ compound by TEM presents a special characteristic that distinguishes it from the rest of the compounds. This compound has the same structure as Nd, Sm, Gd, and Dy compounds, i.e., orthorhombic structure, *Pbnm* SG, with unit cell parameters $\sim a_p\sqrt{2} \times a_p\sqrt{2} \times 2a_p$. The noticeable difference, seen only by TEM in ED patterns and in HREM images, is the presence of nano twin domains (see Figure 7). The experimental ED pattern of Figure 7a can be understood in terms of the superposition of three zone-axis vectors in the orthorhombic structure, $[1\bar{1}0]_o + [110]_o + [001]_o$, that correspond to $[100]_p + [010]_p + [001]_p$ in the frame of a cubic perovskite unit cell. Diffractions, from every region of A, B, and C, were simulated by a Digital Micrograph 3.8.2-Gatan, in the fast Fourier-transformed (FFT) mode. They correspond to nano twin domains with the $\hat{c}$ axis oriented in the three space directions. The size of these nano twin domains varies between 50 and 100 nm. The presence of twin domains in this compound can be attributed to the relationship between cell parameters,

buckling angle distortion (O−M−O), and the rotation φ around $[111]_p$, in the cubic perovskite frame, that is, the rotation of the octahedra defined by the oxygen atoms with the metal ion in the octahedral site. Following the O'Keefe expressions,[15] it is possible to calculate this rotation from the oxygen position[16] giving the lowest value for Pr compound (10.14°) and the largest value for Dy compound (18.78°). The combination of the low value of φ and similar values of cell parameters ($a \sim b \sim c/\sqrt{2} \sim a_p\sqrt{2}$, see Table 1 and Figure 2) for the Pr compound enables perfect matching among the three different twin domains, with the $\hat{c}$ axis following the three space directions. These two conditions are not fulfilled by the structural parameters of the Nd, Sm, Gd, and Dy compounds. Therefore, the twin microstructure is not found. It was emphasized at the beginning of this section that the Pr compound shows an oxygen excess compared with the rest of the Ln compounds. It is possible that this oxygen excess could be located at twin-domain boundaries, as usually found in other perovskite systems.[17−20] Moreover, the existence of dislocation intra-domains and twin dislocations (or dislocations at twin boundaries) from a careful analysis of Figure 7b confirms this suggestion.

(15) O'Keeffe, M.; Hyde, B. G. *Acta Crystallogr., Sect. B* **1977**, *33*, 3802−3813.
(16) Vegas, A.; Vallet-Regí, M.; González-Calbet, J. M.; Alario-Franco, M. A. *Acta Crystallogr., Sect. B* **1986**, *42*, 167−172.
(17) Aguirre, M. H.; Ruiz-Bustos R.; Alario-Franco, M. A. *J. Mater. Chem.* **2003**, *13*, 1156−1160.
(18) Dos Santos-García, A. J.; Aguirre, M. H.; Morán, E.; Sáez Puche, R.; Alario-Franco, M. A. *J. Solid State Chem.* **2006**, *179*, 1296−1302.
(19) Jia, C. L.; Urban, K. *Science* **2004**, *303*, 2001−2004.
(20) Ruiz-Morales, J. C.; Canales-Vázquez, J.; Savaniu, C.; Marrero-López, D.; Zhou, W.; Irvine, J. T. S. *Nature* **2006**, *439*, 568−571.

Conclusions

Single-phase $LnCo_{0.95}Ni_{0.05}O_3$ (Ln = La, Pr, Nd, Sm, Gd, and Dy) compounds were successfully synthesized by a soft chemistry process. This type of synthesis allows one to control the elemental composition and the low level of substitution of Co by Ni. SPXRD and TEM studies performed in Ln compounds are suitable techniques to obtain complementary information about structure and microstructure. The Rietveld refinement of the $LaCo_{0.95}Ni_{0.05}O_3$ compound from SPXRD showed similar fitting parameters for both rhombohedral $R\bar{3}c$ SG and monoclinic $I2/a$ SG. ED studies using the TEM technique revealed that the crystal symmetry of the La compound is better described with a monoclinic $I2/a$ SG than with the rhombohedral $R\bar{3}c$ SG. Ln compounds (Ln = Pr, Nd, Sm, Gd, and Dy) with low-level substitution of Co by Ni have an orthorhombic *Pbnm* structure confirmed by XRD and TEM. The twin domains of the Pr compound did not appear in the other Ln compounds, making $PrCo_{0.95}Ni_{0.05}O_3$ unique among them. This characteristic will influence the transport properties of the material, and further studies are in progress to correlate properties and microstructure.

Acknowledgment. We acknowledge the financial support of the Swiss Federal Office of Energy and the Swiss National Foundation. We thank F. J. García and S. Ebbinghaus for helping us with the synchrotron measurements. We also thank Dr. M. A. Alario-Franco for the use of the facilities at the Microscopy Centre "Luis Brú", UCM-Spain, and the very fruitful TEM discussions.

IC0623821